Aeroacoustic Simulation for Wind Turbine Airfoils

Christof Rautmann[1], Jürgen Dierke[2], Roland Ewert[3], Nils Reiche[4], Nan Hu[5]

DLR AS-TEA, Lilienthalplatz 7, 38108 Braunschweig, Deutschland

[1] *christof.rautmann@dlr.de* , [2] *juergen.dierke@dlr.de* , [3] *roland.ewert@dlr.de* , [4] *nils.reiche@dlr.de* , [5] *nan.hu@dlr.de*

Introduction

Wind energy is one of the major cornerstones in renewable energy production. The amount of turbines and their dimensions have risen steadily over the past decades in order to increase energy production and to fulfill political goals. Beside aesthetic concerns noise emitted from the turbines is a major issue for nearby living people. It was shown in different investigations that wind turbine noise sources can be distinguished into two dominant sources[1, 2]. While the mechanical noise from the nacelle can be treated easily (damping, absorbing material) the aerodynamic noise generated by the outer parts of the rotor blades is still the object of research.
Different airfoil noise mechanisms are known from which the turbulent boundary layer trailing-edge noise (TBL-TEN) has shown to be the most dominating part in modern wind turbine operation. For a low noise airfoil design validated and reliable methods to simulate TBL-TEN are needed. The prediction methods are ranging from rather simple semi-empiric tools (BPM[3]) to complex and resource-intensive scale-resolving simulations.
To overcome this gap the DLR has proposed a hybrid approach consisting of RANS flow simulation combined with stochastic turbulence reconstruction and an acoustic propagation simulation. Several aerodynamic and aeroacoustic properties of the airfoil can be calculated with this procedure in reasonable time of less than one day.

Numerical Setup

A hybrid three step procedure is used to simulate the emitted trailing-edge noise. First, a two-dimensional Reynolds Averaged Navier Stokes (RANS) simulation is conducted to generate the mean flow field around the airfoil. Then, from the RANS turbulence statistics a 4D time and space resolved turbulence field is recreated using the stochastic FRPM (fast random particle mesh) method[4]. In a third step, the fluctuating sound field with turbulent noise sources is simulated using DLRs acoustic propagation code PIANO. The subsequent steps are embedded in an automized tool-chain to generate results for multiple airfoil geometries. The validation of the approach is shown in [5].

CFD

CFD simulations are carried out using the unstructured CFD solver TAU[6]. The simulated mean-flow values and turbulence statistics are then used for the subsequent FRPM and CAA steps.
For each airfoil a two-dimensional computational domain is generated with the outer boundaries extending 100 chord lengths from the airfoil. A hybrid grid is chosen, where the viscous sub-layer is resolved by a structured region and areas far away from the airfoil are resolved by a coarser quad-dominated unstructured grid. The height of the first cell layer at the airfoil surface is determined so, that a dimensionless wall distance of $y^+ < 1$ is achieved. The hybrid structured/unstructured meshing approach reduces cell density in less interesting areas away from the airfoil and cuts the total number of grid cells down to approximately 100k.

FRPM

For the preparation of unsteady vortex sound sources the FRPM method is adopted to force the linearized acoustic perturbation equations in a restricted volume around the trailing-edge (source patch). The Method was first published in 2005[7] and allows to realize time-dependent turbulent fluctuations from averaged turbulent statistics. It generates Gaussian correlated synthetic turbulence of local integral length scale $\Lambda = c_l/C_\mu\sqrt{k_t}/\omega$ ($c_l \simeq 0.5$, $C_\mu = 0.09$), derived from RANS. The linearized fluctuating Lamb vector that occurs as the major vortex-force source term on the right-hand side of the momentum equation (Eq. 2) reads:

$$\boldsymbol{L}' = w(\boldsymbol{x})(\boldsymbol{\omega}_0 \times \mathbf{u}' + \boldsymbol{\omega}' \times \mathbf{u}_0) \ . \qquad (1)$$

In the above given source term $\mathbf{u}_0$ and $\mathbf{u}'$ are the mean and fluctuating velocity that define the unsteady flow velocity via $\boldsymbol{u} = \boldsymbol{u}_0 + \boldsymbol{u}'$. The local source term weighting is represented by $w(\boldsymbol{x})$.It is used to avoid artificial noise by smoothly increasing the source strength towards the trailing-edge. For all test cases a 800 by 240 cells source patch with the dimensions $x/l_c = 0.4$ by $x/l_c = 0.12$ is used. Besides the mean flow velocity $\boldsymbol{u}_0$ the patch contains the turbulence kinetic energy k_t as the variance for the reconstruction of turbulent velocities and the turbulent length scale Λ for the reconstruction.

CAA

The CAA calculations are performed using the DLR code PIANO[8]. In the computational domain the synthetic turbulence is coupled with the CAA solver, which is based on the 4th order accurate DRP scheme proposed by Tam & Webb [9]. Together with the RANS mean-flow the turbulence defines the right-hand side fluctuating source term of the acoustic perturbation equations (APE[10]).
Sound due to the interaction of vorticity with the trailing-edge is generated as part of the CAA simulation step. The vortex dynamics are dominated by linear contributions to the source terms. Non-linear contributions

mainly deemed responsible for sound generation of free turbulent flow are neglected. The APE-4 equation system with neglected entropy and density fluctuations (due to turbulent velocities in low Mach number flows) reads:

$$\begin{aligned} \frac{\partial p'}{\partial t} + c_0^2 \boldsymbol{\nabla} \cdot \left(\rho_0 \boldsymbol{v}' + \boldsymbol{u}_0 \frac{p'}{c_0^2} \right) &= 0 \ , \\ \frac{\partial \boldsymbol{v}'}{\partial t} + \boldsymbol{\nabla} \left(\boldsymbol{u}_0 \cdot \boldsymbol{v}' \right) + \boldsymbol{\nabla} \left(\frac{p'}{\rho_0} \right) &= \boldsymbol{L}' \ . \end{aligned} \tag{2}$$

Quantities with subscript 0 denote mean-flow variables whereas the prime indicates fluctuating quantities. The perturbation velocity is represented by $\boldsymbol{v}'$,the fluctuating acoustic pressure by p' and the fluctuating density by ρ'. The APE are solved on a two-dimensional computational domain extending about 6 by 6 chord lengths with the airfoil in the center. A structured multi-block mesh is chosen to utilize the parallelized computation with PIANO. The CAA mesh consists of 64 blocks with a total number of approximately 1.1 million cells. The far-field region can resolve waves up to $f_{max} = 5\,\mathrm{kHz}$.

Test Cases

For the geometry variation a common wind turbine airfoil - the DU-96-W-180[11] - is chosen and systematically modified in terms of camber and thickness according to the 4-digit NACA scheme[12]. Nine airfoils were created with relative thicknesses of $t/l_c = 0.16, 0.18$ and 0.20 and a mean-line camber of $m/l_c = 0.015, 0.025$ and 0.035. Relative thickness distribution and the position of maximum camber were fixed to the original DU values. The trailing-edge thickness is set to zero for all airfoils.
Attached flow conditions with angles of attack of $\alpha = 3\,^\circ, 4\,^\circ, 5\,^\circ$ and $6\,^\circ$ were chosen. The Reynolds-Number is 3 million and the Mach-Number 0.129. For the later comparison of the noise emission it is essential to compare test cases with matching aerodynamic performances (for example lift coefficient c_L or glide ratios (c_L/c_D)). Additionally, the influence of fixed laminar turbulent transition at the leading edge is investigated.

Results

A total number of 72 combined CFD/CAA simulations was carried out for the different flow and geometry settings. The computational times were around 20 hours per case using a 16CPU cluster node. Beside the aerodynamic coefficients for lift and drag (c_L, c_D) the fluctuating sound pressure p' is recorded over time at 360 virtual microphone positions arranged circular around the trailing-edge in a distance of 2.5 chord lengths. The position directly below the trailing-edge ($x/l_c = 1$, $y/l_c = -2.5$) was chosen for the acoustic evaluation. Figure 1 shows one-third-octave band spectra for the baseline airfoil with varying angle of attack at the desired position. The AoA influence on the trailing-edge noise can be seen. The low-frequency peak around $f \approx 350\,\mathrm{Hz}$ is increased and shifted to lower frequencies while the second (lower) high-frequency peak around $f \approx 2500\,\mathrm{Hz}$ is also increased but shifted towards higher frequencies for increasing angles of attack. This underlines the fact the TBL-TEN spectrum is a result of two independent contributions emanating from the airfoils upper and lower side (see Ref. [3]). The low-frequency peak is thereby caused by the suction side boundary layer and the high frequency peak by the thinner pressure side BL. For further data evaluation the overall sound pressure

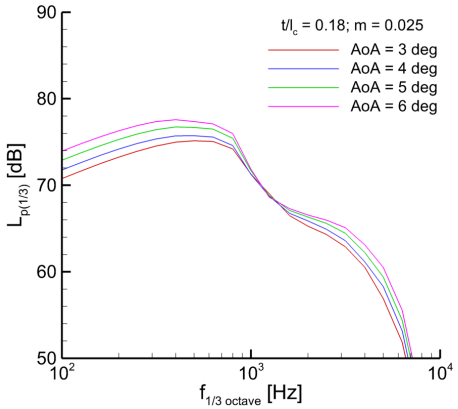

Figure 1: Exemplary one-third-octave band spectra 2.5 chord lengths directly below the trailing-edge.

level $L_{p(OA)}$ (OASPL) was calculated from the one-third-octave band levels to reduce all acoustic information into one value. Such, a combined aeroacoustic aerodynamic analysis based on this value is possible. To judge the airfoils according to their acoustic performance it is essential to do this for the same aerodynamic performance. For example to achieve a certain glide ratio c_L/c_D with minimum noise.
Figure 2 shows overall sound pressure levels compared to glide ratio c_L/c_D for all airfoils under different angles of attack with fixed transition. All airfoils can be operated in a c_L/c_D range between 50 and 90 by adjusting the angle of attack. These aerodynamic performances can be achieved with different noise emissions ranging between 84 dB and 89 dB. While the thin airfoils indicated by the solid lines ($t/l_c = 0.16$) show the smallest overall levels the thick airfoils ($t/l_c = 0.20$) indicated by the dashed-dotted lines show levels which are 3-4 dB higher. For the desired parameter variation of camber and thickness, the airfoil with minimum thickness ($t/l_c = 0.16$) and maximum camber ($m = 0.035$) shows the best performance in terms of glide ratio and overall sound pressure level.

The influence of natural laminar-turbulent flow transition can be seen in figure 3. Beside a reduction in overall levels of about 3-4 dB a gain in glide ratio of about 50 % (mainly due the reduction in c_D) is achieved. So, airfoils sensitive to transition location changes (airfoils designed for long natural laminar flow) are prone to noise increase by upstream transition movement.
Still, the thin strong cambered airfoil ($t/l_c = 0.16$, $m = 0.035$) shows the best performance but a strong dependence on camber reduction can be observed. This can be explained by the fact, that the thin airfoils exhibit a pronounced decrease in laminar running length with angle of attack increase which is additionally amplified by increasing camber.

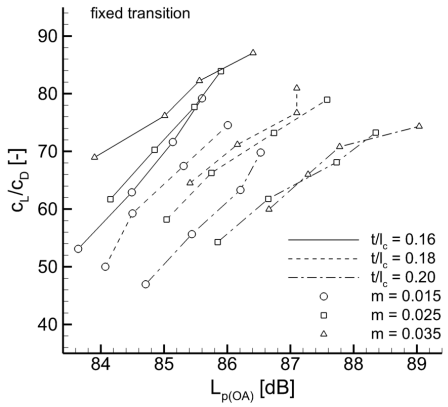

Figure 2: $L_{p(OA)}$ for different geometries and varying angles of attack compared to c_L/c_D (fixed transition)

Further investigations of the test cases have shown that

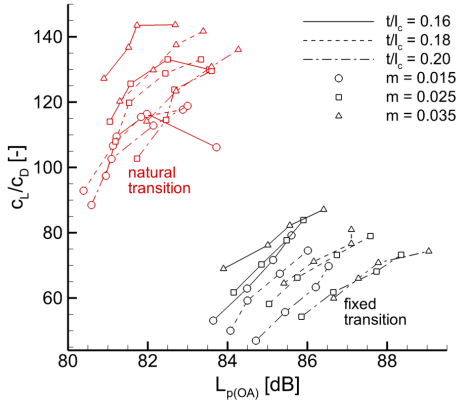

Figure 3: $L_{p(OA)}$ for different geometries and varying angles of attack compared to c_L/c_D (fixed transition)

the thicker suction side boundary layer is mainly responsible for the overall values and precise investigations of boundary layer properties can be very helpful. Generally speaking, reducing boundary layer thickness and turbulent kinetic energy levels in the suction-side trailing-edge region will lead to a better acoustic performance of the airfoil. The interplay with lift and drag generation, as well the influence on transition locations has thereby to be kept in mind.

Conclusion

A precise and fast method for the simulation of airfoil trailing-edge noise was shown. The analysis revealed that it is possible to achieve the same aerodynamic performance (in terms of c_L/c_D ratio) with totally different noise levels with deltas in the range of 5 dB. Moreover, a severe influence of transition locations on noise (around 4 dB) as well as aerodynamic performance was observed. The hybrid CFD/CAA approach is able to predict the noise emission with reasonable accuracy. It can be used for arbitrary geometries and various flow settings and as such represents a valuable tool in the wind turbine rotor blade design process.

Acknowledgments

Major parts of the presented work were performed within the framework of a research collaboration between DLR and Nordex Energy with the aim to develop wind turbine noise prediction methods. The authors thank Nordex Energy for their cooperation and the respective funding.

References

[1] Wagner, S. and Bareiss, R. and Guidati, G.: Wind Turbine Noise. Springer Berlin, 1996

[2] Oerlemans, S. and Sijtsma, P. and Méndez López, B.: Location and quantification of noise sources on a wind turbine. Journal of Sound and Vibration, Vol. 299, No. 4-5, 2007, pp. 779-785

[3] Brooks, T. F., Pope, S. D. and Marcolini, M. A.: Airfoil self-noise and prediction, NASA Refrence Publication 1218, 1989

[4] Ewert, R.: Broadband slat noise prediction based on CAA and stochastic sound sources from a fast random particle-mesh (RPM) method, Computers & Fluids, Vol. 37, 2008, pp 369-387

[5] Rautmann, C., Dierke, J., Ewert, R., Hu, N. and Delfs, J. W.: Generic Airfoil Trailing-Edge Noise Prediction using Stochastic Sound Sources from Synthetic Turbulence, 20th AIAA 2014-3298, 2014

[6] Schwamborn, D., Gerhold, T. and Heinrich, R.: The DLR TAU-Code: Recent Applications in Research and Industry, Proc. of Europ. Conf. on Computational Fluid Dynamics ECCOMAS CFD, 2006

[7] Ewert, R. and Edmunds, R.: CAA Slat Noise Studies Applying Stochastic Sound Sources Based on Solenoidal Digital Filter, AIAA 2005-2862, 2005

[8] Delfs, J. W., Bauer, M., Ewert, R., Grogger, H. A., Lummer, M. and Lauke, T. G. W.: Numerical Simulation of Aerodynamic Noise with DLR's aeroacoustic code PIANO, 2008

[9] Tam, C. and Webb, J.: Dispersion-Relation-Preserving Finite Difference Schemes for Computational Acoustics, Journal of Computational Physics, Vol. 107, 1993, pp. 262–281

[10] Ewert, R.: Acoustic perturbation equations based on flow decomposition via source filtering, Journal of Computational Physics, Vol. 188, No. 2, 2003, pp. 365-398

[11] Timmer, W.A and Rooij, R.P.J.O.M.: Summary of the Delft University Wind Turbine Dedicated Airfoils, 41st Aerospace Sciences Meeting and Exhibit, 2003

[12] Eastman Jacobs, N., Kenneth, E., Ward, E., Pinkerton and Robert M.: The Characteristics of 78 Related Airfoil Sections from Tests in the Variable-density Wind Tunnel, NACA Rept. No. 460, 1933